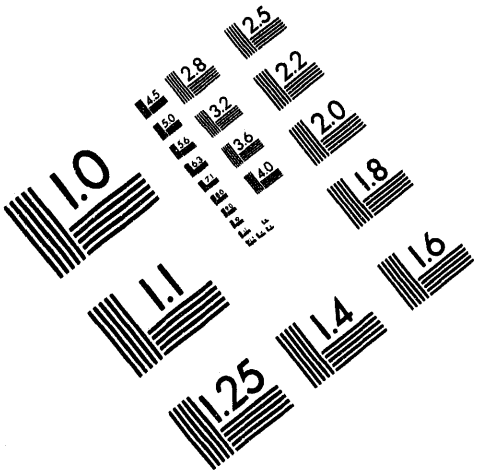

Association for Information and Image Management
1100 Wayne Avenue, Suite 1100
Silver Spring, Maryland 20910
301/587-8202

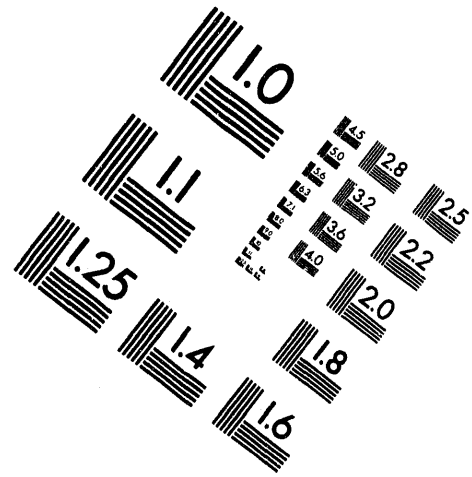

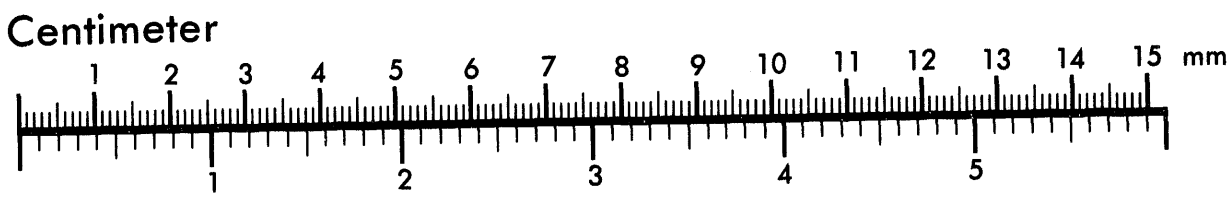

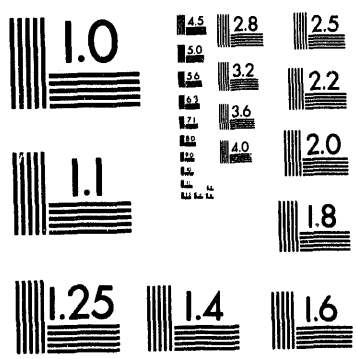

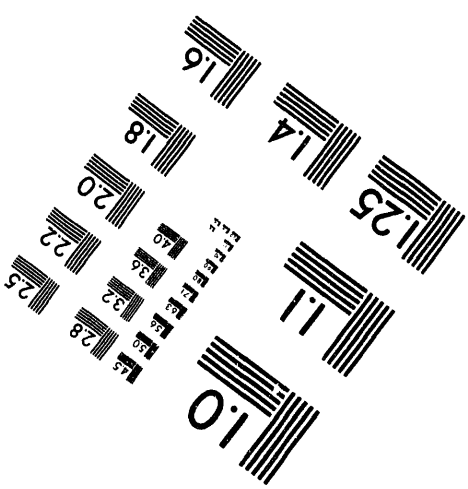

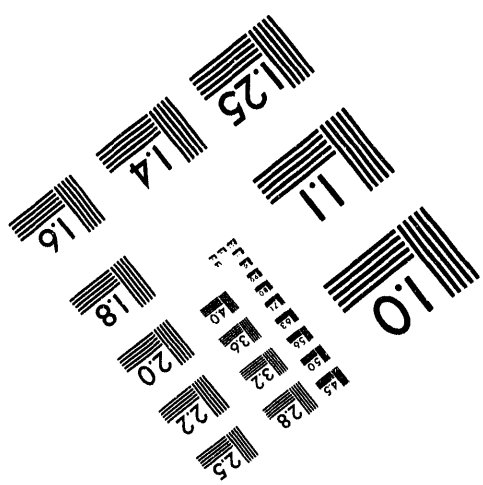

1 of 1

NAVIER-STOKES SIMULATIONS OF WECS AIRFOIL FLOWFIELDS

Gregory F. Homicz

Sandia National Laboratories
Computational Fluid Dynamics Department/Mail Stop 0827
P. O. Box 5800
Albuquerque, NM 87185-0827 USA

ABSTRACT

Sandia National Laboratories has initiated an effort to apply Computational Fluid Dynamics (CFD) to the study of WECS aerodynamics. Preliminary calculations are presented for the flow past a SAND 0018/50 airfoil. The flow solver used is F3D, an implicit, finite-difference code which solves the Thin-Layer Navier-Stokes equations. 2D steady-state calculations are presented at various angles of attack, α. Sectional lift and drag coefficients, as well as surface pressure distributions, are compared with wind tunnel data, and exhibit reasonable agreement at low to moderate angles of attack. At high α, where the airfoil is stalled, a converged solution to the steady-state equations could not be obtained. The flowfield continued to change with successive iterations, which is consistent with the fact that the actual flow is inherently transient, and requires the solution of the full unsteady form of the equations.

NOMENCLATURE

a_∞	freestream speed of sound
e	internal energy
L	characteristic length scale
M_∞	freestream Mach number, U_∞/a_∞
p	static pressure
Re_L	Reynolds number, $\rho_\infty U_\infty L/\mu_\infty$
T	static temperature
U_∞	freestream velocity magnitude, $(u_\infty^2 + w_\infty^2)^{1/2}$
u, v, w	velocity components along x, y, z respectively
x, y, z	cartesian coordinates in physical space
α	angle of attack
γ	specific heat ratio, c_p/c_v
μ	viscosity
ρ	density
ξ, η, ζ	body-fitted coordinate system in computational space

This work was supported by the United States Department of Energy under Contract DE-AC04-94AL85000.

INTRODUCTION

The aerodynamics of Wind Energy Conversion Systems (WECS) is particularly challenging because it involves three-dimensionality, viscous effects, and in many circumstances, significant unsteady phenomena. Present theoretical models can predict with confidence the aerodynamic performance of only those machines that represent incremental departures from earlier, tested designs. The computer models commonly used for such predictions (multiple-streamtube, local circulation, vortex, *etc.*[1]) all rely to some extent on tabulated airfoil characteristics (typically obtained from a wind tunnel test program), and various empiricisms to represent those effects that cannot be simulated directly. Radically different designs typically require extensive experimental testing, followed by code modifications and adjustment of the empiricisms to the new data set. Moreover, blade fatigue life predictions demand even more detailed knowledge of the loads than is presently available from any of the current aerodynamic codes. Computational Fluid Dynamics

DISCLAIMER

(CFD) offers an alternative means of investigating WECS aerodynamics that addresses some of these concerns. CFD distinguishes itself from the semi-analytical theories by its attempt to calculate the relevant flow physics from "first principles", with as little recourse to empiricism as possible. The past few decades have witnessed gains in computer speed and algorithm efficiency that now make it feasible to view CFD as an attractive complement to experimental testing. Though such calculations may still be too time-consuming and expensive for use as production design tools by the WECS community, they can often be performed at considerably less expense than a comprehensive test program. The insight thus gained can ultimately lead to improved models for incorporation into day-to-day design codes.

This paper describes recent efforts at Sandia to apply a suite of previously developed computational tools to the prediction of WECS airfoil flowfields. The next section presents the viscous flow equations and their transformation to computational space. Then the flow solver, F3D, and its capabilities are briefly described. Steady-state solutions are presented for the 2D flow past the SAND 0018/50, an airfoil specifically designed for Vertical-Axis Wind Turbine (VAWT) applications, at various angles of attack. These are believed to be the first Navier-Stokes solutions obtained for this airfoil. The sectional lift and drag coefficients, as well as surface pressure distributions, are validated by comparison with available wind tunnel data.

GOVERNING EQUATIONS

The flow of a compressible, viscous, Newtonian fluid such as air is governed by equations representing the conservation of mass, momentum, and energy, collectively referred to as the Navier-Stokes equations. We will work with a system of normalized variables: all lengths are nondimensionalized by some characteristic length L, velocities by a_∞, time by L/a_∞, density by ρ_∞, pressure by $\rho_\infty a_\infty^2$, temperature by T_∞, energy by a_∞^2, and viscosity by μ_∞. In a fixed frame of reference, using cartesian coordinates (x, y, z), the governing equations can be written in strong conservation form as (see, *e.g.*, Hoffmann[2]):

$$\frac{\partial Q}{\partial t}+\frac{\partial E}{\partial x}+\frac{\partial F}{\partial y}+\frac{\partial G}{\partial z}=\frac{\partial E_v}{\partial x}+\frac{\partial F_v}{\partial y}+\frac{\partial G_v}{\partial z} \tag{1}$$

The boldface quantity Q is the column vector of unknown variables, and E, F, and G are known as the inviscid flux vectors:

$$Q=\begin{bmatrix}\rho\\ \rho u\\ \rho v\\ \rho w\\ \rho e_t\end{bmatrix} \quad E=\begin{bmatrix}\rho u\\ \rho u^2+p\\ \rho uv\\ \rho uw\\ (\rho e_t+p)u\end{bmatrix} \quad F=\begin{bmatrix}\rho v\\ \rho vu\\ \rho v^2+p\\ \rho vw\\ (\rho e_t+p)v\end{bmatrix} \quad G=\begin{bmatrix}\rho w\\ \rho wu\\ \rho wv\\ \rho w^2+p\\ (\rho e_t+p)w\end{bmatrix} \tag{2}$$

Here e_t is the total energy/unit mass, $e_t = e + (1/2)\left(u^2+v^2+w^2\right) = c_v T + (1/2)\left(u^2+v^2+w^2\right)$. E_v, F_v, and G_v represent the viscous flux vectors:

$$E_v=\begin{bmatrix}0\\ \tau_{xx}\\ \tau_{xy}\\ \tau_{xz}\\ u\tau_{xx}+v\tau_{xy}+w\tau_{xz}-q_x\end{bmatrix} \quad F_v=\begin{bmatrix}0\\ \tau_{yx}\\ \tau_{yy}\\ \tau_{yz}\\ u\tau_{yx}+v\tau_{yy}+w\tau_{yz}-q_y\end{bmatrix} \quad G_v=\begin{bmatrix}0\\ \tau_{zx}\\ \tau_{zy}\\ \tau_{zz}\\ u\tau_{zx}+v\tau_{zy}+w\tau_{zz}-q_z\end{bmatrix} \tag{3}$$

$[\tau]$ and $\vec{q}$ represent the symmetric stress tensor and heat flux vector, whose elements are given respectively by, *e.g.*,

$$\tau_{xy} = \tau_{yx} = \frac{1}{Re_L}\left[\mu\left(\frac{\partial u}{\partial y}+\frac{\partial v}{\partial x}\right)\right] \qquad q_x = \frac{\mu}{Re_L Pr\,(\gamma-1)\,M_\infty^2}\frac{\partial T}{\partial x} \tag{4}$$

By considering the 1st ... 5th elements in the above column vectors, Eq. (1) is seen to express the conservation equations of mass, x-momentum, y-momentum, z-momentum, and energy, respectively.

For flows bounded by curvilinear surfaces, which do not lie conveniently along x, y, or z = constant, the imposition of boundary conditions on Eq. (1) is very difficult in cartesian coordinates. To get around this, the equations are transformed from *physical space* (x, y, z, t) to a boundary-conforming *computational space* (ξ, η, ζ, τ). In general, the transformation must be performed numerically, rather than analytically, and serves two purposes. First, the originally curvilinear flow domain is mapped into one which is rectangular (planar in 2D, or a "box" in 3D), and thus ideally suited for the use of an equally-spaced cartesian grid in (ξ, η, ζ). Secondly, surfaces on which boundary conditions are to be imposed will, *by definition*, lie along a surface of either ξ, η, or ζ = constant. This will become clearer when the airfoil and grid are discussed below.

When the above equations are transformed to computational space, after much manipulation they can still be written in strong-conservation form similar to Eq. (1):

$$\frac{\partial \hat{Q}}{\partial \tau}+\frac{\partial \hat{E}}{\partial \xi}+\frac{\partial \hat{F}}{\partial \eta}+\frac{\partial \hat{G}}{\partial \zeta} = \frac{\partial \hat{E}_v}{\partial \xi}+\frac{\partial \hat{F}_v}{\partial \eta}+\frac{\partial \hat{G}_v}{\partial \zeta} \tag{5}$$

The transformed vector of unknowns is given by $[\hat{Q}] = [Q]/J$, where J is the *Jacobian* of the transformation. The expressions for J, the transformed inviscid flux vectors, $\hat{E}$ ..., and the viscous flux vectors, $\hat{E}_v$ ..., are somewhat lengthy, and as they are reported elsewhere[2], will not be repeated here.

CODE DESCRIPTION

The system of partial differential equations represented by Eq. (5) is far too complex to solve analytically except for the most trivial of cases. The computer code used to generate the results reported here is F3D, a program developed by Professor Joseph Steger and several colleagues and students[3]-[7]. For high *Re* flows, the effects of viscosity are often confined to relatively thin shear layers adjacent to the surface. Assuming that ζ is the coordinate normal to the surface in computational space, it can be argued that the viscous terms in ξ and η will be much smaller than those in ζ, and hence can be neglected. F3D solves the resulting system, termed the Thin-Layer Navier-Stokes (TLNS) equations. Of course, care must be exercised in applying such a system to flows involving massive separation and/or recirculation, where the underlying assumptions may not hold. F3D has been successfully used to predict the aerodynamics of subsonic, transonic and supersonic flowfields[5]-[7], including viscous flows at large incidence[5].

Solution Algorithm

An evenly-spaced, cartesian grid of discrete points is overlaid on the flow in (ξ, η, ζ) space, and the partial derivatives in the equations are approximated by finite differences. For added numerical stability, a flux-split upwind differencing scheme is applied to the convective terms in ξ, while central differences are retained in η and ζ. The resulting system of algebraic equations is second-order accurate in space, and first- or second-order accurate in time. It can be inverted using a two-factor, implicit, approximate-factorization algorithm which is both stable and relatively efficient[5]. An explicit algorithm is available as an option. To facilitate application to complex geometries, multi-block grids, both overlapping and embedded, can be accommodated. F3D can be used to study flows which are either two- or three-dimensional, steady or unsteady, inviscid (Euler) or viscous, and laminar or turbulent.

Turbulence & Transition

Strictly speaking, the equations discussed above apply only to laminar flows. At high *Re*, the flow can be expected to transition to turbulence. This introduces additional diffusive terms into the equations termed turbulence shear stresses, or more usually, *Reynolds stresses*. The Reynolds stresses represent additional unknowns, and the system of equations becomes underdetermined.

At this point recourse is made to empiricism, in the form of a *turbulence model*. Turbulence models provide the additional relations required to close the system of equations. The results reported here were generated using the Baldwin-Lomax algebraic turbulence model[8]. At the risk of over-simplifying, it postulates that the effects of turbulence may be modeled by solving the laminar flow equations (Eq. (5) above) with the molecular viscosity, μ, replaced by an effective viscosity, $\mu_{eff} = \mu + \mu_t$. μ_t is the so-called *eddy viscosity* arising from turbulence. Algebraic relations are used to relate μ_t to the mean flow variables in $[Q]$; typically $\mu_t \gg \mu$, as turbulent mixing is much more efficient than viscous (*i.e.*, laminar) diffusion. Details can be found in Ref. [8].

Transition from laminar to turbulent flow is still very much an active area of research. For practical calculations it is necessary to resort to empiricism or experimental knowledge of its location. F3D was modified so that transition locations could be independently input on both the upper and lower airfoil surfaces. Upstream of these points the flow was treated as fully laminar ($\mu_t = 0$), and downstream it was assumed to be fully turbulent. Limited experimental data are available on the transition locations for the SAND 0018/50 from the work of Reda[9]. These locations were used as input to F3D; specific values will be mentioned in connection with the numerical results below.

AIRFOIL & GRID

FIGURE 1. SAND 0018/50 AIRFOIL

The SAND 0018/50 was designed to have characteristics favoring its application to the Darrieus Vertical-Axis Wind Turbine (VAWT)[10], and is currently in use on the Sandia 34-m Test Bed in Bushland, Texas[11]. Its profile is shown in Fig. 1. It is a symmetric, 18% thickness-to-chord ratio section designed to maintain laminar flow over ~ 50% of chord at zero angle of attack. The resulting lower drag improves its performance at low-to-moderate windspeeds. It also has an abrupt-stall characteristic; this is advantageous in high winds, where passive stall regulation is used to limit output power.

The grid used in this study was generated using the Eagle grid generation code developed at Mississippi State University[12]. Figure 2 shows the grid transformation in schematic form. The airfoil lies in the (x, z) plane in physical space (Fig. 2a), where it forms the inner boundary of the flow domain; the outer boundary is chosen to be a circle. The region between them is mapped to a rectangle in the (ξ, ζ) plane in

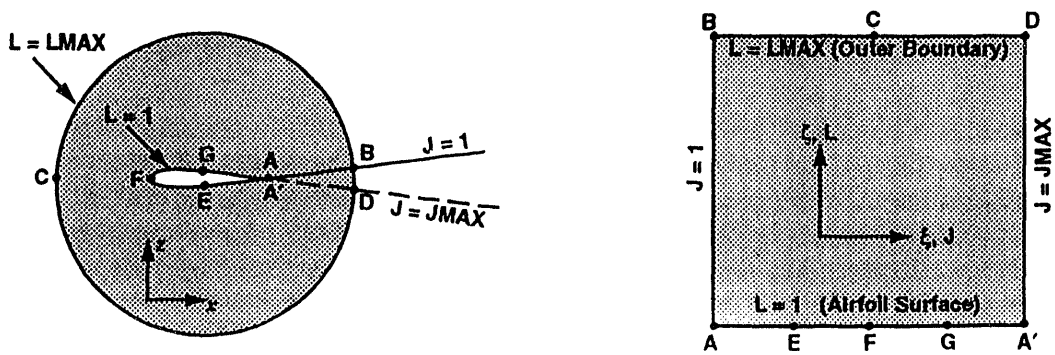

(a) Physical Space (b) Computational Space

FIGURE 2. SCHEMATIC OF 2D AIRFOIL MAPPING (not to scale)

computational space (Fig. 2b). The points labelled **A...G** show that the airfoil is mapped to the bottom of the rectangle, and the outer boundary to the top.

Figure 3a shows an overall view of the actual grid, which is an "O-type" structured grid that wraps circumferentially around the airfoil. JMAX = 201 grid lines were used in the circumferential (J or ξ) direction, and LMAX = 110 were used in the radial (L or ζ) direction. Uniform freestream conditions are imposed on the outer boundary, which has a radius of ~ 100*c* (*c* being one chord length). This large radius was chosen in an attempt to simulate as nearly as possible "unconfined" flow conditions. At this scale the airfoil itself, at the center of the grid, is not visible.

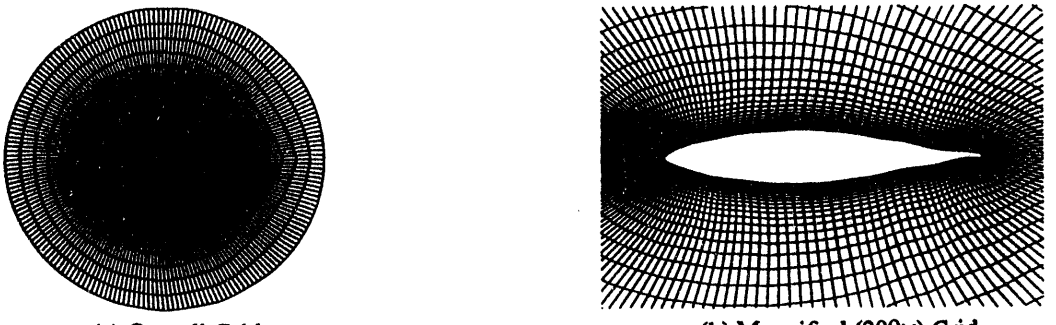

(a) Overall Grid (b) Magnified (200×) Grid

FIGURE 3. FINITE DIFFERENCE GRID FOR SAND 0018/50

In Fig. 3b the view is magnified ~ 200 times for a better look at the grid in the vicinity of the airfoil. Grid points are packed much more tightly in the vicinity of the airfoil, so as to resolve the very thin boundary layers which occur at high *Re*. In units of chord length, the thickness of the first row of grid cells adjacent to the airfoil, $\Delta n/c$, is on the order of 10^{-7}. With 201 points circumferentially, the *average* grid spacing in the streamwise direction, $\Delta s/c$, is about 10^{-2}. However, as can be seen in Fig. 3b, the points were also clustered near the leading and trailing edges, where $\Delta s/c \sim 10^{-4}$ and 10^{-3}, respectively. These values were chosen based on the results of the grid-refinement studies of Zingg[13]. On the airfoil surface, "no-slip" boundary conditions were imposed, *i.e.*, $u = w = 0$.

RESULTS & DISCUSSION

Preliminary calculations were run for the SAND 0018/50 at three different angles of attack: 4°, 10°, and 20°, chosen to see how the code performed in various flow regimes. At 4° one would expect the flow to remain attached, with the airfoil on the linear portion of its lift characteristic; $\alpha = 10°$ is just below the angle at which the airfoil stalls; and at 20° the airfoil is deeply stalled. Experimental wind tunnel data for the sectional lift and drag coefficients, C_L, $C_D = (L, D) / \left(1/2\rho_\infty U_\infty^2 c \right)$, as well as the surface pressure coefficient, $c_p = (p - p_\infty) / \left(1/2\rho_\infty U_\infty^2 \right)$, were available for comparison.

$\alpha = 4°$

The first case considered had freestream conditions of $M_\infty = 0.26$, $Re_c = 1.5 \times 10^6$, and $\alpha = 4°$. These conditions correspond to those for Run No. 4193 in Ref. [14]. Based on Reda's flow visualization studies[9], the transition locations were set at $x/c = 0.65$ and 0.70 on the upper(suction) and lower(pressure) surfaces, respectively. The convergence of C_L and C_D with respect to iteration number is shown in Fig. 4a below. Note that the values of C_D have all been multiplied by a factor of 10 to allow visualization on the same scale with C_L. After 3000 iterations the computed C_L had settled down to a value of 0.510, *vs.* the experimentally measured 0.40, a difference of +27%. The predicted C_D was 0.0118, also +27% higher than the measured value of 0.0093. At this low angle of attack, the contributions to C_D from pressure and skin friction are comparable. This underscores the need to use very tightly clustered grids near the airfoil surface, to allow better resolution of the wall shear stress.

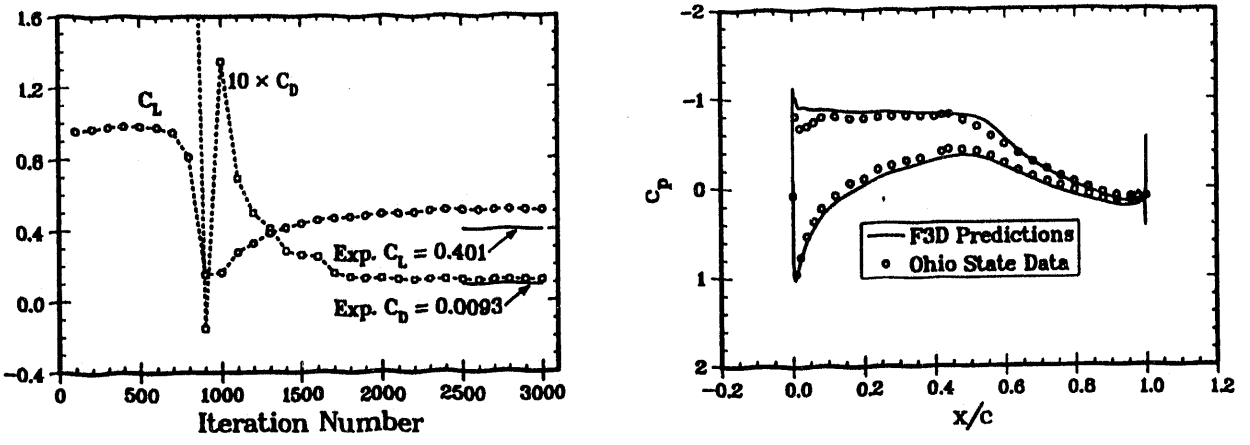

(a) C_L, C_D Convergence History

(b) Surface Pressure Coefficient, c_p

FIGURE 4. COMPARISON OF C_L, C_D AND c_P WITH MEASURED DATA FOR THE SAND 0018/50 AT $M_\infty = 0.26$, $Re_C = 1.5 \times 10^6$, $\alpha = 4°$

Figure 4b compares the predicted surface pressure coefficients against the measured data. Note that the vertical axis has been inverted so that the upper portion of the curve corresponds to the upper (suction) surface of the airfoil, and the lower portion to the lower (pressure) surface. The agreement is reasonably good, with the biggest difference occurring near the leading edge on the upper surface. Over most of the airfoil, the pressure is overpredicted on the lower side, and underpredicted on the upper side, which explains why the calculated C_L was too high.

The computed streamline pattern is shown in Fig. 5a. The airfoil chord is horizontal, with the flow entering at a 4° angle from the lower left. As expected, the flow remains attached to the airfoil with no evidence of separation. Figure 5b displays the contours of static pressure in the surrounding flowfield. This is a gray-scale reproduction of the full-color original, with each color corresponding to a different level of p/p_∞, as indicated by the color bar on the right. The stagnation point lies just below the nose of the airfoil. The much lower pressures on the upper surface, as compared with those on the lower side, are of course responsible for the lift.

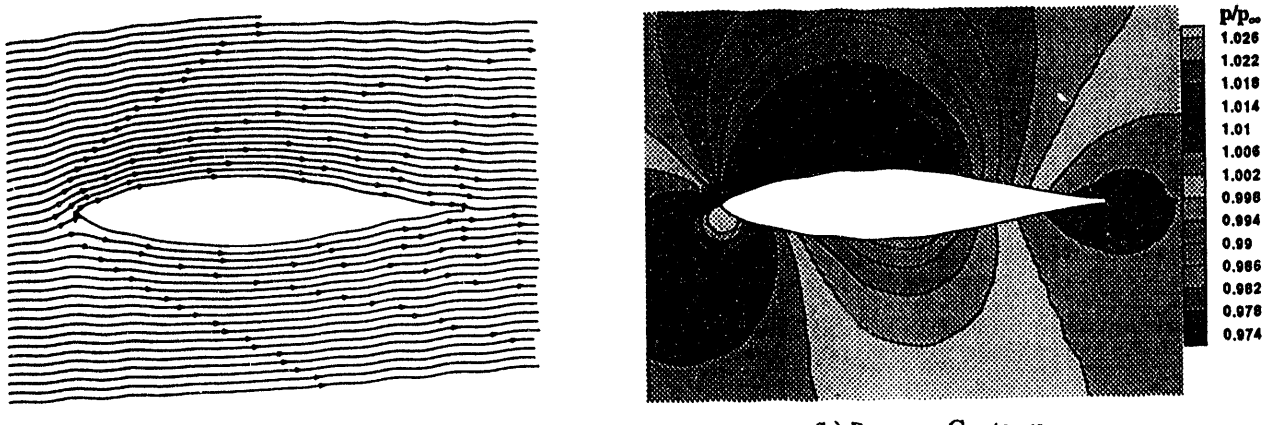

(a) Streamline Pattern

(b) Pressure Contours

FIGURE 5. COMPUTED FLOWFIELD FOR THE SAND 0018/50 AT $M_\infty = 0.26$, $Re_C = 1.5 \times 10^6$, $\alpha = 4°$

$\alpha = 10°$

The next case run was for $M_\infty = 0.21$, $Re_c = 1.19 \times 10^6$, and $\alpha = 10°$, corresponding to Run No. 731 in Ref. [14]. Transition was specified at the leading edge on the upper surface, and at $x/c = 0.79$ on the lower surface[9]. The convergence history of C_L and C_D is shown in Fig. 6a. The L_2–norm, essentially the r.m.s.

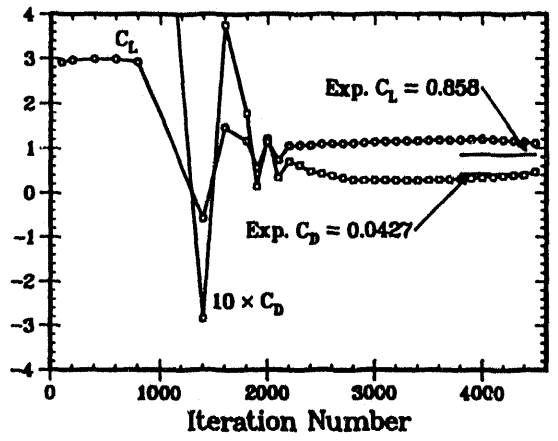

(a) C_L, C_D Convergence History

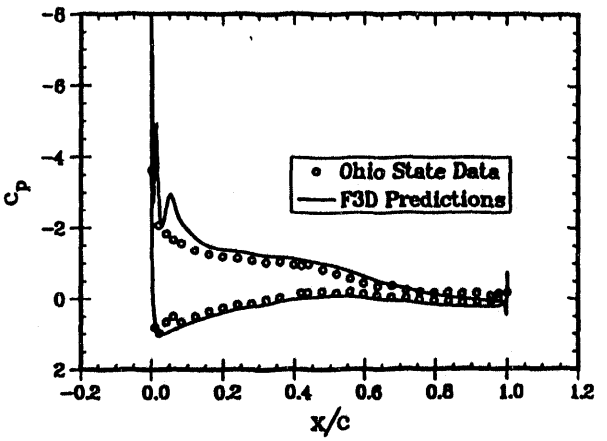

(b) Surface Pressure Coefficient, c_p

FIGURE 6. COMPARISON OF C_L, C_D AND c_P WITH MEASURED DATA FOR THE SAND 0018/50 AT $M_\infty = 0.21$, $Re_C = 1.19 \times 10^6$, $\alpha = 10°$

value of $[\Delta\hat{Q}]$ between successive iterations, is monitored as an overall measure of convergence. By iteration 3000 or so, this had only dropped by a little more than an order of magnitude from its peak. Generally, a drop of two to three orders of magnitude is considered necessary for adequate convergence. For this reason the calculation was continued and after 4500 iterations it had fallen more than two orders of magnitude. The predicted force coefficients were $C_L = 1.102$ *vs.* the measured 0.858 (+28%), and $C_D = 0.0467$ *vs.* the measured 0.0427 (+9%). The surface pressure distributions are compared in Fig. 6b. Over most of the chord the agreement is reasonably good. As was the case at 4°, the code appears to generally overestimate pressures on the lower surface, and underestimate them on the upper, which is again consistent with the predicted C_L being high. However, near the leading edge on the suction surface there are two "spikes" in the predicted pressures not present in the data. More will be said about these shortly.

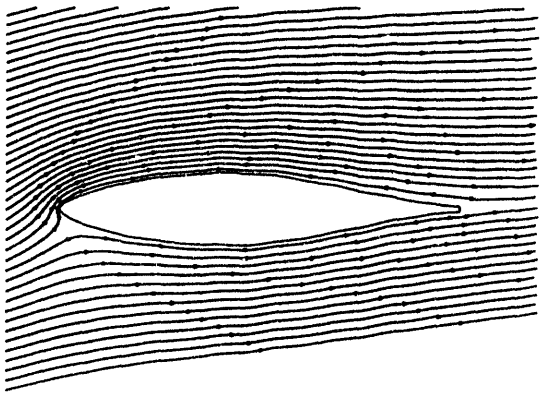

(a) Overall View

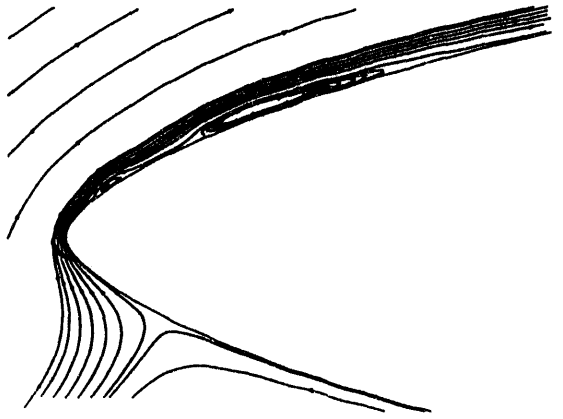

(b) Magnified View

FIGURE 7. STREAMLINE PATTERN FOR THE SAND 0018/50 AT $M_\infty = 0.21$, $Re_C = 1.19 \times 10^6$, AND $\alpha = 10°$

Figure 7a shows the streamline pattern for this flow. The stagnation point has moved further down on the lower surface, relative to that in Fig. 5a. Though the flow remains largely attached, the first streamline above the upper surface does not follow the surface as closely as it did at 4°. As there appears to be some "waviness" near the leading edge, this region was greatly magnified, resulting in the view shown in Fig. 7b. Several additional streamlines were interpolated adjacent to the surface to better illuminate the flow pattern. Two separation/reattachment bubbles are now evident on the suction surface. One would expect lower pressures there, and indeed, these bubbles correspond in location to the negative "spikes" in the predicted surface pressures in Fig. 6b. It was found that the bubbles' location and size, as well as the height of the spikes, varied somewhat during the calculation, though C_L and C_D were changing only slightly. These oscillations are taken as evidence of incipient separation from the vicinity of the leading edge. Whether such bubbles occurred in the experiment is unknown, though the smooth pressure variation in Fig. 6b would seem to argue against it. On the other hand, the pressure instrumentation used to obtain the data in Fig. 6b did not have a particularly fast response time[15], and so in some sense those data represent a time-averaged response which may have masked such behavior.

The predicted pressure contours are shown in Fig. 8. At this magnification, the negative pressure spikes near the leading edge noted above are not visible. The same color bar was used here as was used in Fig. 5b, to facilitate comparing the two. The contours are qualitatively similar to those at 4°, except that the pressures on the bottom are generally higher, and the low pressure region on the suction side extends out further into the flow. This is consistent with the higher lift achieved at this angle of attack.

FIGURE 8. PRESSURE CONTOURS FOR SAND 0018/50 AT $M_\infty = 0.21$, Re_C

$\alpha = 20°$

The last case attempted was for $M_\infty = 0.2$, $Re_c = 1.8 \times 10^6$, and $\alpha = 20°$. These conditions unfortunately did not admit a converged solution. C_L, C_D, and the L_2–norm never stopped oscillating, and eventually the calculation "blew up". The surface pressure distribution, streamline pattern, and pressure field contours also exhibited significant variation as the iterations proceeded. Figure 9 displays a typical streamline pattern; it is strongly suggestive of the massive separation and vortex shedding phenomena associated with a stalled airfoil. The patterns at other stages in the calculations are qualitatively similar, though the location of the vortical elements changes. Though care should be taken not to read too much into unconverged solutions, as they do not satisfy the governing equations, this strongly suggests that at 20° the flowfield is inherently transient, and characterized by massive separation and vortex shedding. This is consistent with the observation made earlier, that at this α the airfoil is known to be deeply stalled. Such flows require that all the unsteady terms in the governing equations be retained. Though F3D is capable of treating such cases, this greatly increases computing times, and no such calculations have been attempted as yet.

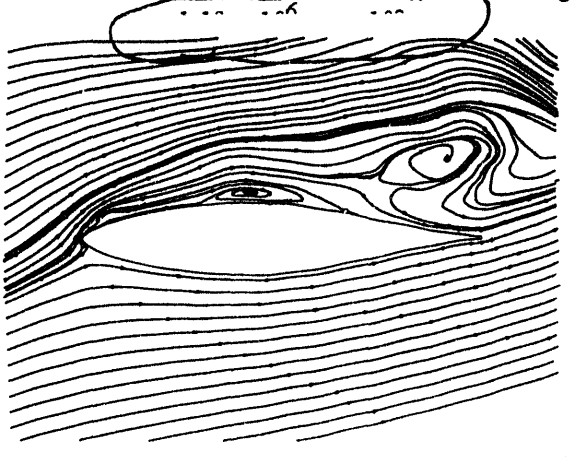

FIGURE 9. STREAMLINE PATTERN FOR SAND 0018/50 AT $M_\infty = 0.2$, $Re_C = 1.8 \times 10^6$, $\alpha = 20°$ (not converged)

Timing Statistics

It is reasonable to ask what level of resources, in terms of both hardware and computer time, are required to perform such calculations. The above cases were run either on a Cray Y-MP8/864, a Sun SPARC 10/MODEL 30, or a SPARC 10/MODEL 51 desktop workstation, using 64-bit arithmetic; this corresponds to single-precision on the Cray and double-precision on the SPARC 10s. Table 1 shows the CPU time required to perform 100 iterations, the CPU time/(iteration–grid-pt.), and the total CPU time required to perform the approximately 3500 iterations typically needed for a converged steady-state solution. (The latter figure is probably conservative.) The times quoted are only approximate, and may vary by 10-15% depending on the particular run. The last row also assumes a calculation begun with uniform freestream properties everywhere in the flow. Convergence is possible in considerably fewer iterations by starting the calculation from an earlier, converged, solution for conditions close to those desired.

TABLE 1. STEADY–STATE AIRFOIL CALCULATION CPU TIMES

Platform:	Cray Y-MP	Sun SPARC 10/30	Sun SPARC 10/51
Per 100 iterations	15 min	115 min	80 min
Per iter./per grid pt.	4.1×10^{-4} sec	3.1×10^{-3} sec	2.2×10^{-3} sec
Converged solution	8.8 hrs	67 hrs	47 hrs

SUMMARY & CONCLUSIONS

Numerical simulations based on the TLNS equations have been performed for the flow past the SAND 0018/50 airfoil using the finite-difference code F3D. Steady-state solutions have been attempted at angles of attack of 4°, 10°, and 20°. Surface pressures agree reasonably well with the data over most of the chord at 4° and 10°. Predicted values of C_L and C_D are high by about 25-30%. C_L is largely the result of (inviscid) pressure forces, and hence should exhibit a smaller error; why it does not remains a matter of investigation. C_D is more difficult to predict than C_L because of the contribution from skin friction, particularly at lower α's. More study is needed regarding the effects of grid resolution, the turbulence model used, and the assumed transition locations on C_D.

The steady-state calculations would not converge for $\alpha = 20°$, where the 0018/50 is known to be deeply stalled. The computed streamline patterns were consistent with this, and suggest that such flows must be simulated with the unsteady terms included. Future plans call for trying to simulate the 0018/50's response while undergoing sinusoidal oscillations in pitch, for which experimental data have also been obtained[14].

These results indicate that while CFD holds much promise for improving our understanding of WECS flowfields, we are a long way from being able to predict their aerodynamics without any recourse to empiricism or wind tunnel data. The phenomena of turbulence and transition, in particular, produce effects which presently must be modeled rather than directly simulated. While the time required for such calculations may currently prevent their use in day-to-day design activities, the continual improvements in desktop computer power and algorithm efficiency can be expected to lead to progressively more sophisticated engineering codes.

ACKNOWLEDGMENTS

This work was supported by the Wind Energy Technology Department at Sandia National Laboratories. The author wishes to acknowledge numerous technical discussions with Dr. Dale Berg of that department. He is also deeply indebted to Dr. Daniel Barnette, currently in the Parallel Computational Sciences Department; without his early development efforts and guidance in the use of F3D, this work would not have been possible.

REFERENCES

1. Strickland, J.H., "A Review of Aerodynamic Analysis Methods for the Vertical-Axis Wind Turbine," *Proceedings of the 5th ASME Wind Energy Symp.*, New Orleans, LA, February 23–26, 1986, pp. 7–17.

2. Hoffmann, K.A., *Computational Fluid Dynamics for Engineers*, published by Engineering Education System, Austin, TX, 1989.

3. Pulliam, T.H. and Steger, J.L., "Implicit Finite-Difference Simulations of Three-Dimensional Compressible Flow," *AIAA Journal*, Vol. 18, No. 2, February 1980, pp. 159–167.

4. Steger, J.L. and Warming, R.F., "Flux Vector Splitting of the Inviscid Gasdynamic Equations with Application to Finite-Difference Methods," *Journal of Computational Physics*, Vol. 40, No. 2, April 1981, pp. 263–293.

5. Ying, S.X., Steger, J.L., Schiff, L.B., and Baganoff, D., *Numerical Simulation of Unsteady, Viscous, High Angle of Attack Flows Using a Partially Flux-Split Algorithm*, AIAA Paper 86–2179, presented at AIAA 13th Atmospheric Flight Mechanics Conference, Williamsburg, VA, August 18–20, 1986.

6. Steger, J.L., Ying, S.X., and Schiff, L.B., "A Partially Flux-Split Algorithm for Numerical Simulation of Compressible Inviscid and Viscous Flow," *Proceedings of the Workshop on Computational Fluid Dynamics*, Institute of Nonlinear Sciences, University of California, Davis, CA, 1986.

7. Buning, P.G., Chiu, I.T., Obayashi, S., Rizk, Y.M., and Steger, J.L., "Numerical Simulation of the Integrated Space Shuttle Vehicle in Ascent," AIAA Paper 88-4359, *Proceedings of the AIAA Atmospheric Flight Mechanics Conf.*, Minneapolis, MN, August 15–17, 1988, pp. 265-283.

8. Baldwin, B.S. and Lomax, H., *Thin Layer Approximation and Algebraic Model for Separated Turbulent Flows*, AIAA Paper 78–257, presented at the AIAA 16th Aerospace Sciences Meeting, Huntsville, AL, January 16–18, 1978.

9. Reda, D.C., "Observations of Dynamic Stall Phenomena Using Liquid Crystal Coatings," *AIAA Journal*, Vol. 29, No. 2, February 1991, pp. 308–310.

10. Gregorek, G.M. and Klimas, P.C., "Tailored Airfoils for Wind Turbine Applications," *Proceedings of the 6th ASME Wind Energy Symposium*, Dallas, TX, February 15–18, 1987.

11. Berg, D.E. and Ashwill, T.D., "An Update on the Structural Design of the Sandia 34-m Vertical-Axis Wind Turbine," *Proceedings of the 5th ASME Wind Energy Symposium*, New Orleans, LA, February 23–26, 1986.

12. Anonymous, *Eagle User Manual, Vol. 1: Introduction and Grid Applications; Vol. 2: Surface Generation Code; Vol. 3: Grid Generation Code*, Mississippi State University, Mississippi State, MS, 1988.

13. Zingg, D.W., "Grid Studies for Thin-Layer Navier-Stokes Computations of Airfoil Flowfields," *AIAA Journal*, Vol. 30, No. 10, October 1992, pp. 2561–2564.

14. Gregorek, G.M., Hoffmann, M.J. and Berchak, M.J., *Steady-State and Oscillatory Aerodynamic Characteristics of a Sandia 0018/50 Airfoil*, Data Report, Aeronautical and Astronautical Research Laboratory, Ohio State University, Columbus, OH, August, 1989.

15. Hoffmann, M.J., Aeronautical and Astronautical Research Laboratory, Ohio State University, Columbus, OH, private communication.

DATE
FILMED
7/12/94

END